Electromagnetic Fluctuations during Fast Reconnection in a Laboratory Plasma

Hantao Ji, Stephen Terry, Masaaki Yamada, Russell Kulsrud, Aleksey Kuritsyn, and Yang Ren
Princeton Plasma Physics Laboratory, Princeton University, P.O. Box 451, Princeton, New Jersey 08543, USA
(Received 29 January 2003; published 18 March 2004)

Experimental evidence for a positive correlation is established between the magnitude of electromagnetic fluctuations up to the lower-hybrid frequency range and enhancement of reconnection rates in a well-controlled laboratory plasma. The fluctuations belong to the right-hand polarized whistler wave branch, propagating obliquely to the reconnecting magnetic field, with a phase velocity comparable to the relative drift velocity between electrons and ions. The measured short coherence lengths indicate their strongly nonlinear nature.

DOI: 10.1103/PhysRevLett.92.115001 PACS numbers: 52.35.Vd, 52.35.Qz, 52.35.Ra, 52.72.+v

Magnetic reconnection [e.g., [1]] plays an important role in determining the evolution of magnetic topology in relaxation processes in high-temperature laboratory plasmas, magnetospheric substorms, solar flares, and more distant astrophysical plasmas. Often, magnetic reconnection is invoked to explain the observed rapid release of magnetic energy in these highly conducting plasmas. A central question concerns why the observed reconnection rates are much faster than predictions by the Sweet-Parker model [2,3] based on two-dimensional (2D) magnetohydrodynamics (MHD) with the Spitzer resistivity. The extremely small resistivity causes the magnetic field to dissipate only in very thin current sheets, which impede the mass outflow and thus limit the reconnection rate. The subsequently proposed Petschek model [4] is based on slow shocks that open up the outflow channel allowing larger mass flows and thus the faster reconnection rates. However, it was shown later [5,6] that the Petschek solution is not compatible with uniform or smooth resistivity profiles. On the other hand, perhaps not surprisingly, resistivity can be enhanced by microinstabilities active only in the reconnection region where plenty of free energy exists in the form of a large relative drift between ions and electrons and large inhomogeneities in pressure. This anomalous resistivity increases the reconnection rate, and its localization also reestablishes Petschek-like solutions [6–8]. Alternatively, a recent theory [9] attempts to explain fast reconnection rates based on nondissipative terms, notably the Hall term, in the generalized Ohm's law in a 2D and laminar fashion.

The underlying microinstabilities [1] for the resistivity enhancement have been considered to be predominantly electrostatic due to their effectiveness in wave-particle interactions. The primary candidate is the lower-hybrid drift instability (LHDI) [10], which is frequently observed in space [11]. Recently, this instability has been studied in relation with reconnection in laboratory [12] and space [13,14]. The main conclusion is that the LHDI is present only in the low-β edge region of the current sheet, but *not* in the high-β central region, where the resistivity needs to be enhanced. This is consistent with an earlier theory [15] on stabilization of LHDI by finite β, and also with recent numerical simulations [16,17].

By contrast, much less attention has been paid to (electro)magnetic fluctuations and their relation with reconnection, although they are also regularly observed in space [11,13]. Here we report the first experimental evidence for magnetic fluctuations up to the lower-hybrid frequency range during fast reconnection in a well-controlled laboratory plasma, the magnetic reconnection experiment (MRX) [18]. Earlier experiments [19] indicated evidence for high-frequency magnetic fluctuations in the electron MHD regime where only electrons are magnetized, but their role in the reconnection process was unclear. However, most plasmas of interest for the reconnection problem are well into the MHD regime where ions are also magnetized at least outside of the reconnection region, as in MRX. Other ongoing reconnection experiments [20] focus on dynamics in lower frequencies.

In the MRX, magnetic reconnection is induced by reducing toroidal currents in two flux cores whose axisymmetric shape ensures the *global* 2D geometry (Fig. 1). The reconnecting field component, B_Z, is pulled together radially, forming a current sheet flowing along the θ direction. All essential parameters are measured by an extensive set of diagnostics [18]. Previously, it was shown [21] that the observed reconnection rates can be explained by a modified Sweet-Parker model including an

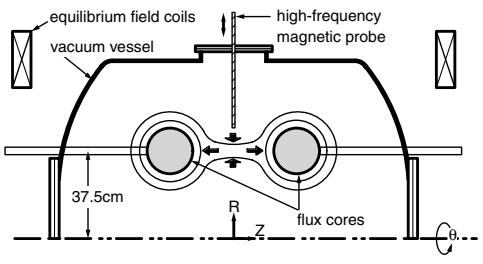

FIG. 1. Experimental setup in MRX. The reconnecting magnetic field component is in the Z direction and resultant current sheet flows in the θ direction. Inflow and outflow are in the R (radial) and Z directions, respectively.

effective resistivity, determined experimentally by $\eta^* \equiv E_\theta/j_\theta$, where E_θ and j_θ are the toroidal reconnecting electric field and current density, respectively. When the collisionality is high η^* is very close to the Spitzer perpendicular resistivity η_{Spitzer}. When the collisionality is reduced $\eta^* \gg \eta_{\text{Spitzer}}$. High-frequency fluctuations have been measured in MRX to study possible resistivity enhancement due to microinstabilities in low collisionality regimes. Although the LHDI electrostatic fluctuations were identified at the low-β edge region of the current sheet, they did not temporally and spatially correlate with the reconnection process nor did their collisionality dependence. This leads to the conclusion that the electrostatic fluctuations do not play an essential role in the fast reconnection at MRX [12,22].

The experimental results reported here focus on magnetic fluctuations, which correlate well with the fast reconnection. The main diagnostics used are four small pickup coils (1.25 mm diameter) mounted within a small volume of $3 \times 3 \times 3$ mm^3 inside an electrostatically shielded glass tube (5 mm diameter) measuring all three magnetic components. The outputs are fed into a miniature circuit board embedded in the probe shaft near the tip to provide noise immunity and impedance matching. The effective bandwidth is up to 30 MHz. The experiments were performed during "null-helicity" reconnection [18], where the third component B_θ is typically mall compared to the upstream reconnecting component just outside the current sheet, B_Z^{up}. At the axial location ($Z = 0$) where the majority of the measurements were made, B_θ typically decreases from a magnitude comparable to B_Z^{up} in earlier times ($t \lesssim 270$ μs) to $\ll B_Z^{\text{up}}$ after $t \sim 270$ μs.

Typical raw signals during a single discharge are shown in Fig. 2. High-frequency fluctuations in all three components are detected when the current sheet moves close to the probe, and then persist as long as the reconnection continues. Spectrograms, which display the fluctuation power in the time-frequency domain, are also shown in Fig. 2. The spectra appear to be broadband, sometimes with distinct peaks, extending up to the lower-hybrid frequency $f_{\text{LH}} \equiv \sqrt{f_{\text{ce}} f_{\text{ci}}}$ (since ion plasma frequency $f_{\text{pi}} \gg \sqrt{f_{\text{ce}} f_{\text{ci}}}$) based on B_Z^{up}. The fluctuations peak near the current sheet center with $|\tilde{\boldsymbol{B}}|/B_Z^{\text{up}}$ up to 5% (Fig. 3).

Propagation characteristics are measured by two independent techniques at the current sheet edge ($R = 40$ cm) during the earlier times (260 μs $\leq t \leq$ 270 μs) when the fluctuations are relatively small (Fig. 3) and coherent. The hodogram technique is based on the tip trajectories of a fluctuating magnetic field vector measured at a spatial point [19]. At a given frequency, the condition $\boldsymbol{\nabla} \cdot \tilde{\boldsymbol{B}} = 0$ is translated to $\boldsymbol{k} \cdot \tilde{\boldsymbol{B}} = 0$, where $\boldsymbol{k}$ is the dominant wave number vector. Then the direction of $\boldsymbol{k}$ (or $-\boldsymbol{k}$) can be determined by $\tilde{\boldsymbol{B}}(t_0) \times \tilde{\boldsymbol{B}}(t_0 + \delta t)$ with the sign ambiguity resolved by the phase shift measurements (see later). It is found that majority of waves propagate approximately

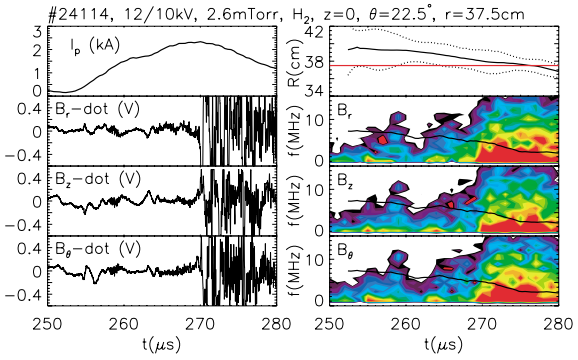

FIG. 2 (color). Traces of typical raw signals during reconnection represented by plasma current (top left panel). Spectrograms are shown on the lower-right panels where fluctuation powers are color coded (decreasing power by order of red, yellow, green, blue, and white) in the time-frequency domain. The black lines indicate f_{LH} based on B_Z^{up}. The top right panel displays locations of the probe (red line) and the current sheet (center as black solid line and edges as dashed lines). When the current sheet center moves close to the probe, high-frequency magnetic fluctuations are detected.

in the $-\theta$ direction, along which electrons drift. Since the background magnetic field vector $\boldsymbol{B}_0$ at this particular location and time has comparable B_Z and B_θ components, the waves propagate obliquely to $\boldsymbol{B}_0$. This can be seen in the power spectra constructed in the domain of frequency and the angle between $\boldsymbol{k}$ and $\boldsymbol{B}_0$ [Fig. 4 (left)]. Most waves propagate with angles smaller than 90° (~30° to ~60° with varying spreads depending on frequency), consistent with right-hand polarized fast (whistler) waves when $f > f_{\text{ci}}$ [23]. We note that the measured radial component of $\boldsymbol{k}$ is small, consistent with a standing wavelike structure across the current sheet (also see Fig. 3). Therefore, it is concluded that the observed magnetic fluctuations are right-hand polarized whistlerlike waves propagating obliquely to the magnetic field while remaining trapped within the current sheet.

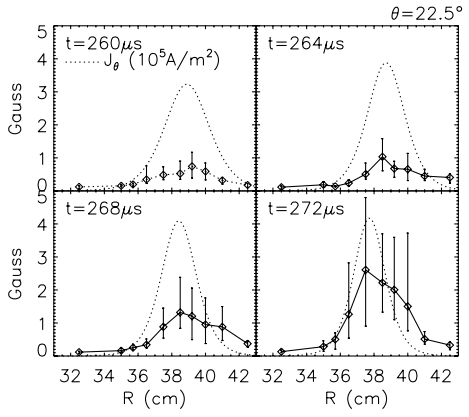

FIG. 3. Radial profile of total amplitude (averaged over about ten discharges at each spatial point) of magnetic fluctuations with $f \geq 1$ MHz at four times. The current density profiles (dotted lines) are shown for reference.

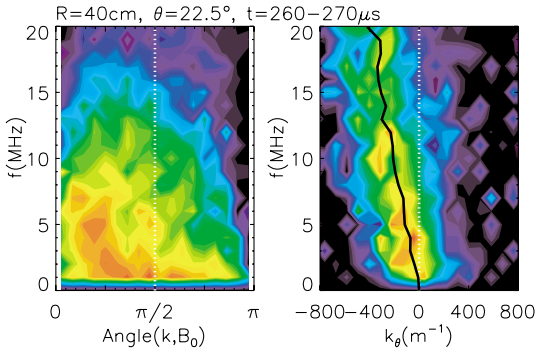

FIG. 4 (color). Power spectra (color coded as in Fig. 2) for $\tilde{\boldsymbol{B}}$ in the domain of frequency and the angle between dominant $\boldsymbol{k}$ and $\boldsymbol{B}_0$ (left) and for $\tilde{\boldsymbol{B}}_Z$ in the domain of frequency and k_θ (right) at $R = 40$ cm and $t = 260$–270 μs. Each spectrum uses more than 40 discharges.

While the direction of $\boldsymbol{k}$ is determined by the hodogram technique, its magnitude or the wavelength is determined by a second technique using the phase shift measured between two spatial points along the θ or Z direction at the same radius ($R = 40$ cm) and time ($260\ \mu\text{s} \leq t \leq 270\ \mu\text{s}$). Two glass tubes, each containing a pickup coil, are mounted with a distance of 7 mm between their axes. Each signal is fed to a single-channel version of the miniature in-shaft amplifier [12]. The power spectra are constructed in the domain of (f, k_θ) [Fig. 4 (right)] or (f, k_Z) (not shown). It is found that the phase velocity is mainly in the $-\theta$ direction with a magnitude of $V_{\text{ph}} \simeq \omega/k_\theta = (3.4 \pm 0.8) \times 10^5$ m/s [from the slope of the black line in Fig. 4 (right)], reasonably consistent with the relative drift velocity $V_{\text{d}} \equiv j_\theta/en = (2.5 \pm 0.9) \times 10^5$ m/s, where n is the density.

When the amplitudes are large, as at the current sheet center or late in the discharge ($t \gtrsim 270\ \mu$s), the measurements of $\boldsymbol{k}$ have not been as successful due to extremely short coherence lengths. The coherence $|\tilde{B}_1\tilde{B}_2^*|/(|\tilde{B}_1||\tilde{B}_2|)$ between signals $\tilde{B}_1$ and $\tilde{B}_2$ rapidly decreases to the noise level when the separation is larger than 0.5–1.5 cm, suggesting their strongly nonlinear nature. [For comparison, the wavelength estimated from Fig. 4 (right) is $\sim$3 cm for $f = 10$ MHz.] Furthermore, it is found that the fluctuation amplitude varies substantially along the toroidal direction, breaking the 2D axisymmetry.

The observed magnetic fluctuations cannot be simply interpreted as byproducts of LHDI as attempted in space observations [13] since essentially no electrostatic fluctuations are detected concurrently. In addition, theoretically, magnetic fluctuations due to LHDI are dominated by their component along $\boldsymbol{B}_0$ and propagate primarily across $\boldsymbol{B}_0$ while experimentally all three components have roughly the same amplitude (see Fig. 2) propagating obliquely to $\boldsymbol{B}_0$. The waves are not whistler waves driven by electron temperature anisotropy [1] because these propagate mainly along $\boldsymbol{B}_0$.

Many observed key features of the magnetic fluctuations, however, are consistent with the so-called modified two-stream instability (MTSI) at high β [10,24,25]. Theoretically, in contrast to LHDI, MTSI is driven only by a large relative drift across the magnetic field in *homogeneous* plasmas. At low β, both LHDI and MTSI behave similarly. When β is large ($\gtrsim 1$), LHDI is stabilized [15] while MTSI remains unstable but with the Alfvén speed V_{A} replacing the ion sound (or thermal) speed as the critical drift speed. The resultant waves are largely magnetic and right-hand polarized, obliquely propagating whistlerlike waves with $V_{\text{ph}} \sim V_{\text{d}}$ [24]. When $\beta \gtrsim 1$ and $V_{\text{d}}/V_{\text{A}} \gtrsim 5$ as in MRX, the waves are unstable only at certain propagation angles to the field [25]. Localization of magnetic fluctuations to the high-β region at the current sheet center is consistent with recent global eigenmode analyses [26,27].

The next important question concerns how the observed magnetic fluctuations are related to the resistivity enhancement, and thus the fast reconnection process. It is found that the fluctuation amplitudes are sensitive to plasma density or equivalently collisionality. When the density is reduced from $\sim 5 \times 10^{19}$ m^{-3} to $\sim 2 \times 10^{18}$ m^{-3}, $|\tilde{\boldsymbol{B}}_Z|$ increases from 0.1 G (close to the noise level for the measurements) to $\sim$1 G, as shown in Fig. 5 (left). Since the resistivity enhancement also strongly depends on the collisionality [21], a positive correlation between magnetic fluctuations and resistivity enhancement is established, as shown in Fig. 5 (right) [28]. In addition, there exists experimental evidence for local nonclassical electron heating (Fig. 6) since with fast parallel energy flow the Ohmic heating can explain only up to about 20% of the observed temperature peaking in the current sheet [29]. The remaining electron heating can be thought of as due to a frictional interaction between electrons and waves, analogous to the usual Ohmic heating where momentum is transferred from electrons to ions while both are heated.

Quantitative estimates of resistivity enhancement due to these fully nonlinear waves, however, are not straightforward. Momentum per unit volume carried by electromagnetic waves is $\boldsymbol{k}\mathcal{E}/\omega$, where $\mathcal{E} \approx 2(|\tilde{\boldsymbol{B}}|^2/2\mu_0)$ is the total wave energy density. The wave momentum increases at the rate 2γ where γ is the linear growth rate of the

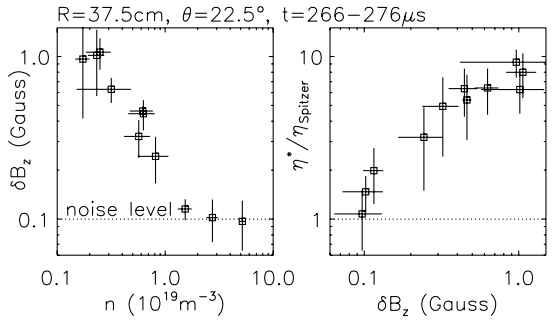

FIG. 5. $\tilde{\boldsymbol{B}}_Z$ amplitude versus density measured by Langmuir probe (left) and resistivity enhancement (right) at the current sheet center.

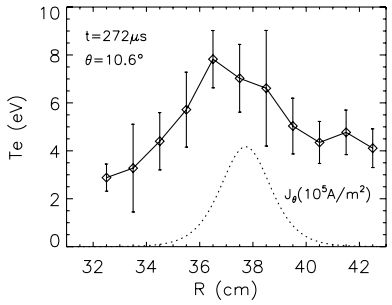

FIG. 6. Radial profile of electron temperature measured by Langmuir probes. The current density profile (dotted line) is shown for reference.

waves. Taking the ion rest frame, $\gamma = \gamma_e + \gamma_i$, where $\gamma_e (> 0)$ is due to wave growth by electrons and $\gamma_i (< 0)$ is due to wave damping on ions. The loss of momentum of the electrons to the waves (at the rate of $2\gamma_e$) is a force that is equivalent to an effective electric field E_θ^{wave}, where

$$enE_\theta^{\text{wave}} = 2k_\theta(|\tilde{B}|^2/\mu_0)(\gamma_e/\omega). \quad (1)$$

When the waves saturate, there is a nonlinear damping rate, $\gamma_{\text{NL}} (< 0)$, so that $\gamma_e + \gamma_i + \gamma_{\text{NL}} = 0$. Equation (1) remains unchanged when the nonlinear damping is mainly on the ions, which is likely [30]. [If, however, the nonlinear damping is on the electrons then γ_e needs to be replaced by $\gamma_e + \gamma_{\text{NL}} = -\gamma_i (> 0)$.] Assuming $\gamma_e \sim \omega$ since the waves are highly nonlinear and taking $|\tilde{B}| = 2.5$ G (Fig. 3) and $n = 2 \times 10^{18}\ \text{m}^{-3}$, one finds that $E_\theta^{\text{waves}} \sim 0.3(k_\theta/\text{m}^{-1})$ V/m. Therefore a value of $k_\theta \gtrsim 300\ \text{m}^{-1}$ or a toroidal wavelength of $\lesssim 2$ cm is sufficient to produce a force on the electrons that balances the reconnection field, $\langle E_\theta \rangle \sim 100$ V/m. The fact that the required wavelength is comparable to the measured toroidal coherence lengths suggests that the waves could play a significant role during fast reconnection. Obviously, a more quantitative understanding requires further experimental and theoretical effort, such as investigating the nonlinear effects and the scaling dependence suggested by Fig. 5.

In summary, a detailed experimental study in MRX has established, for the first time, a positive correlation between magnetic fluctuations up to the f_{LH} range and fast reconnection. The waves are identified as right-hand polarized whistler waves, propagating obliquely to the reconnecting field, with $V_{\text{ph}} \sim V_{\text{d}}$. These waves are consistent with the electromagnetic MTSI driven by drift speeds large compared to the Alfvén speed at high β. The short coherence lengths indicate their strongly nonlinear nature. Interestingly, many of these observed features resemble those measured in the previous electron MHD experiments [19], in contrast to a more recent study [31], which claims importance of electrostatic fluctuations. Close comparative studies with these and other experiments, space observations, and theories and simulations using proper models and boundary conditions should provide much-needed physical insight.

The authors are grateful to D. Cylinder and R. Cutler for their technical support, and J. Whitney, K. Shen, J. Carter, and T. Carter for their contributions. This work was supported by DOE, NASA, and NSF.

[1] D. Biskamp, *Magnetic Reconnection in Plasmas* (Cambridge University Press, Cambridge, England, 2000).
[2] P. Sweet, in *Electromagnetic Phenomena in Cosmical Physics*, edited by B. Lehnert (Cambridge University Press, New York, 1958), p. 123.
[3] E. Parker, J. Geophys. Res. **62**, 509 (1957).
[4] H. Petschek, NASA Spec. Publ. **50**, 425 (1964).
[5] D. Biskamp, Phys. Fluids **29**, 1520 (1986).
[6] R. Kulsrud, Earth Planets Space **53**, 417 (2001).
[7] M. Ugai and T. Tsuda, J. Plasma Phys. **17**, 337 (1977).
[8] D. Biskamp and E. Schwarz, Phys. Plasmas **8**, 4729 (2001).
[9] J. Birn *et al.*, J. Geophys. Res. **106**, 3715 (2001).
[10] N. Krall and P. Liewer, Phys. Rev. A **4**, 2094 (1971).
[11] D. Gurnett *et al.*, J. Geophys. Res. **81**, 6059 (1976).
[12] T. Carter *et al.*, Phys. Rev. Lett. **88**, 015001 (2002).
[13] I. Shinohara *et al.*, J. Geophys. Res. **103**, 20 365 (1998).
[14] S. Bale *et al.*, Geophys. Res. Lett. **29**, 2180 (2002).
[15] R. Davidson *et al.*, Phys. Fluids **20**, 301 (1977).
[16] R. Horiuchi and T. Sato, Phys. Plasmas **6**, 4565 (1999).
[17] G. Lapenta and J. Brackbill, Phys. Plasmas **9**, 1544 (2002).
[18] M. Yamada *et al.*, Phys. Plasmas **4**, 1936 (1997).
[19] W. Gekelman and R. Stenzel, J. Geophys. Res. **89**, 2715 (1984).
[20] Y. Ono *et al.*, Phys. Rev. Lett. **76**, 3328 (1996); M. Brown *et al.*, Astrophys. J. **577**, L63 (2002); J. Egedal *et al.*, Phys. Rev. Lett. **90**, 135003 (2003); N. Crocker *et al.*, Phys. Rev. Lett. **90**, 035003 (2003).
[21] H. Ji *et al.*, Phys. Rev. Lett. **80**, 3256 (1998).
[22] T. Carter *et al.*, Phys. Plasmas **9**, 3272 (2002).
[23] T. Stix, *Waves in Plasmas* (American Institute of Physics, New York, 1992).
[24] D.W. Ross, Phys. Fluids **13**, 746 (1970).
[25] C. Wu *et al.*, Phys. Fluids **26**, 1259 (1983).
[26] P. Yoon *et al.*, Phys. Plasmas **9**, 1526 (2002).
[27] W. Daughton, Phys. Plasmas **10**, 3103 (2003).
[28] In order to correctly calculate the averaged reconnecting toroidal electric field, $\langle E_\theta \rangle$, with toroidal asymmetry, we have performed an extensive scan over 20 toroidal angles to map out $B_Z(R, \theta, t)$ at $Z = 0$. The poloidal flux $\Psi(t)$ contained within the reconnecting toroidal neutral line (where $B_Z = 0$) is calculated through spatial integration. Then $\langle E_\theta \rangle$ is obtained by dividing $\partial\Psi(t)/\partial t$ by the total length of the neutral line. The averaged resistivity obtained by this method is reasonably consistent with values based on the axisymmetry assumption provided a sufficient number of discharges are used for averaging.
[29] H. Ji *et al.* (to be published).
[30] E. Choueiri, Phys. Plasmas **6**, 2290 (1999).
[31] R. Stenzel *et al.*, Phys. Plasmas **10**, 2810 (2003).